The prion hypothesis applied to the τ protein in Alzheimer's Disease using Graph Theory

Case Study in Mathematical Modelling

Candidate Number: 1081169

Abstract. Prions are misfolded proteins that induce neurodegenerative diseases in mammals by acting as a template and misfolding other proteins. τ proteins are believed to act in this way with Alzheimer's Disease. This paper aims to modelling the spreading of misfolded τ proteins using the brain connectome — a graph of neural connections in the brain — starting with the Fisher KPP reaction-diffusion model as a baseline. Different mechanisms (clearance and damage) are then considered and incorporated into the model in order to understand their role and relevance. This understanding plays a key role for developing future treatments for this seemingly unstoppable disease.

1 INTRODUCTION AND BIOLOGICAL BACKGROUND

Alzheimer's Disease (AD) is a neurodegenerative disorder characterised by dementia. It significantly alters memory function and causes functional impairment without affecting the state of consciousness. According to the Alzheimer's Disease International, there were more than 55 million people suffering from it in the year 2020, and its impact is expected to double every 20 years [1].

The prion-like spreading of AD has been under the consideration of the neuroscientific community for some decades [2]. Prions are proteins that act as infectious agents, causing a lethal neurodegeneration throughout mammalian brains. The prion hypothesis, backed by experimental evidence, provides a framework that explains the way that proteins become infectious and how they spread and self-replicate. The infectiousness emerges as a consequence of the misfolding of said proteins. Once misfolded, they can spread and infect the rest of the brain through self-replication: healthy proteins can adopt the infectious misfolding from toxic ones [3].

The first speculations regarded the Amyloid β (Aβ) protein as the one causing the brain damage [4]. However, given that (i) no therapeutical progress has been made with regard to this hypothesis, and (ii) the levels of misfolded τ proteins have been noticed to increase during the progress of AD [5], this study will model the spread of τ proteins. Aβ propagates through the extracellular matrix while τ spreads within axonal pathways, and transport through the axonal pathways can be accurately represented by the weighted graph modelling neural connections provided by the Human Connectome Project [6]. This study will use the lowest-resolution connectome, consisting of 83 nodes, to simulate the τ protein spreading throughout the brain.

Modelling the spread of the misfolded τ proteins is of high interest: tracking how each cerebral region gets infected can help towards a more profound understanding of the evolution of Alzheimer's. Heiko Braak [7] already studied the progression of AD classifying it into 6 stages, which we will refer to as Braak stages. These can be associated with certain brain regions, allowing us to classify most nodes into one of the 6 Braak stages. From Braak's study we know that misfolded τ proteins are initially found in the transentorhinal region of the temporal lobe.

We will begin by considering the Fisher-Kolmogorov-Petroski-Piskunov (Fisher-KPP for short) reaction-diffusion equation [8, 9]. After implementing the model and analysing the results, we will move onto a model proposed in [10] where τ concentration and the brain clearance are coupled. This is an improvement compared to

the Fisher-KPP model given that the latter does not account for the brain clearance mechanisms that remove toxic proteins. Experimental evidence suggests that these clearance mechanisms are deteriorated with the presence of toxic proteins, providing the motivation behind coupling both processes. However, the exact dependence of the clearance on the toxic concentration is still being investigated [10–12]. Finally, we will explore how brain damage can be included in the model to study the impact it has. Cognitive damage adversely affects the neural connections between nodes, which can be translated to the Connectome framework by altering the entries of the weighted graph.

2 FISHER-KPP MODEL

2.1 REACTION-DIFFUSION EQUATION

The Fisher-KPP equation is a basic nonlinear reaction-diffusion equation. When applied to our case, as done in [13], the variable to solve for will be p, the concentration of misfolded τ proteins:

$$\frac{\mathrm{d}p}{\mathrm{d}t} = \nabla \cdot (\mathbf{D} \cdot \nabla p) + \alpha p\,(1-p)\,, \tag{1}$$

where the first term of the RHS accounts for transport, $\mathbf{D}$ being the diffusion tensor, and the second term models the interactions between healthy and misfolded τ proteins. Notice this second term is a nonlinear logistic term with a carrying capacity of 1 and a rate α. Hence, in this model the concentration p is nondimensionalised in a way that it belongs to the interval $[0, 1]$.

Using the Connectome, we can model diffusion in the following way. Subtracting the degree matrix from the weighted adjacency matrix gives the Graph Laplacian, which captures the connectivity of each node relative to its neighbours: $\mathbf{L} = \mathbf{D_1} - \mathbf{W}$. The weighted degree matrix $\mathbf{D_1}$ is a diagonal matrix whose element (i, i) is defined as:

$$(\mathbf{D_1})_{ii} = \sum_{j=1}^{83} W_{ij}. \tag{2}$$

Now, the Human Connectome Project provides several ways of defining the weighted adjacency matrix, all of them already nondimensionalised. The simplest defines the entry (i, j) as just the number of axons or nerve fibres n connecting nodes i and j: $\mathbf{W}_{ij} = n_{ij}$. The other definitions also depend on the average length between those nodes l_{ij}. The possibilities include $\mathbf{W}_{ij} = n_{ij}/l_{ij}$ and $\mathbf{W}_{ij} = n_{ij}/l_{ij}^2$. We will use the

last one, where the connectivity between two nodes is significantly penalised if they are a long distance from each other. The Graph Laplacian is therefore:

$$\mathbf{L} = \begin{pmatrix} \sum_{j=1}^{83} \frac{n_{1j}}{l_{1j}^2} - \frac{n_{11}}{l_{11}^2} & -\frac{n_{12}}{l_{12}^2} & \cdots \\ -\frac{n_{21}}{l_{21}^2} & \sum_{j=1}^{83} \frac{n_{2j}}{l_{2j}^2} - \frac{n_{22}}{l_{22}^2} & \cdots \\ \vdots & \vdots & \ddots \end{pmatrix}. \tag{3}$$

Note that $n_{ij} = n_{ji}$ and $l_{ij} = l_{ji}$, as they represent the same physical quantity (number or length of fibres joining two nodes). Hence, the Graph Laplacian will be symmetric.

The Graph Laplacian, whose values represent the connectivity between neighbouring nodes, can now be used to rewrite Equation (1) as a matrix-vector ODE. Now the variable to solve for will be a vector of the τ protein concentrations in each node $\vec{p} = (p_1, p_2, \ldots, p_{83})^T$:

$$\frac{\mathrm{d}\vec{p}}{\mathrm{d}t} = -\rho_1 \mathbf{L}\vec{p} + \alpha\vec{p} \odot \left(\vec{1} - \vec{p}\right), \tag{4}$$

where ρ is an effective diffusion coefficient and $\odot$ is used to represent element-wise, or Hadamard, multiplication. An ODE for every node i can be inferred from Equation (4):

$$\frac{\mathrm{d}p_i}{\mathrm{d}t} = -\rho \sum_{j=1}^{83} L_{ij} p_j + \alpha p_i \left(1 - p_i\right). \tag{5}$$

However, Equation (5) as it is implies a nonphysical diffusion process. Within this process, we know that the total mass of misfolded τ proteins, $M = \sum_{i=1}^{83} p_i v_i$, should be conserved, where if p_i is adimensional, v_i should too. Thus, we can consider the volumes v_i to be normalised by a factor or norm of 1 unit volume, so that they are now adimensional but keep their values. We will later explain why this is reasonable. It can be ratified that mass is not being conserved by the diffusion term by calculating the mass rate using Equation (5) while considering only diffusion and forgetting about the conversion term as follows:

$$\frac{\mathrm{d}M}{\mathrm{d}t} = \frac{\mathrm{d}}{\mathrm{d}t} \sum_{i=1}^{83} p_i v_i = \sum_{i=1}^{83} \frac{\mathrm{d}p_i}{\mathrm{d}t} v_i = -\rho \sum_{i=1}^{83} \sum_{j=1}^{83} L_{ij} p_j v_i = -\rho \sum_{j=1}^{83} p_j \sum_{i=1}^{83} L_{ij} v_i \neq 0, \tag{6}$$

assuming the volumes v_i are constant. This calculation confirms that the process of diffusion has some nonzero mass rate, which is unphysical. However, Equation (3) implies that $\sum_{i=0}^{83} L_{ij} = 0 \ \forall j$. Therefore, if the v_i in Equation (6) was not present, we would indeed get a 0 mass rate, making the transport process physical again. In other words, dividing the transport term by v_i ensures mass is conserved. However, note that if the transport term is divided by the volumes, ρ also scales the volumes.

Therefore, it is not only a diffusion coefficient, now it also accounts for the volume normalisation. This is the reason why considering a normalisation by a factor of one is reasonable: ρ will absorb the actual normalisation factor. Fortunately, the volumes of each node are available from the Connectome. To account for this then, we reach the final form for this initial Fisher-KPP model:

$$\frac{\mathrm{d}p_i}{\mathrm{d}t} = -\rho \sum_{j=1}^{83} \frac{L_{ij} p_j}{v_i} + \alpha p_i (1 - p_i), \tag{7a}$$

$$p_i(0) = p_{i,0}. \tag{7b}$$

Note the diffusion term does now yield $\frac{\mathrm{d}M}{\mathrm{d}t} = 0$.

2.2 COMPUTATIONAL IMPLEMENTATION

The subsequent analysis and results come from the model in Equation (7) being implemented in Python using the Numpy library. It is solved following an explicit scheme discretising time, and the diffusion through the brain is modelled using the Connectome's Graph Laplacian as an array.

We know that misfolded τ proteins start accumulating in the transentorhinal region [7]. Therefore, only those nodes associated with Braak stage I have a nonzero initial concentration seeding. The toxic proteins reach the rest of the brain through diffusion, producing the succession of the following Braak stages.

2.3 TRANSPORT VS REACTION

The values for ρ and α, the coefficients scaling the diffusion and the misfolding rates, can be chosen by studying the system's evolution for different relative sizes.

Figure (1) shows the average concentration of all nodes grouped by Braak stages for two cases: (i) diffusion dominates over the concentration growth due to conversion in the left graph, i.e., $\rho/\alpha \gg 1$, and (ii) growth dominates over diffusion in the right one, i.e., $\rho/\alpha \ll 1$.

We can observe that if diffusion dominates the toxic proteins are able to reach all brain regions before growing in numbers, resulting in an almost simultaneous increase of the concentration for all brain regions. Only the nodes associated with the Braak stage I get infected at a slightly earlier time, which is just the effect of the initial seeding location. This behaviour contradicts the findings of Heiko Braak in [7]: we know different regions are saturated by misfolded τ proteins at different

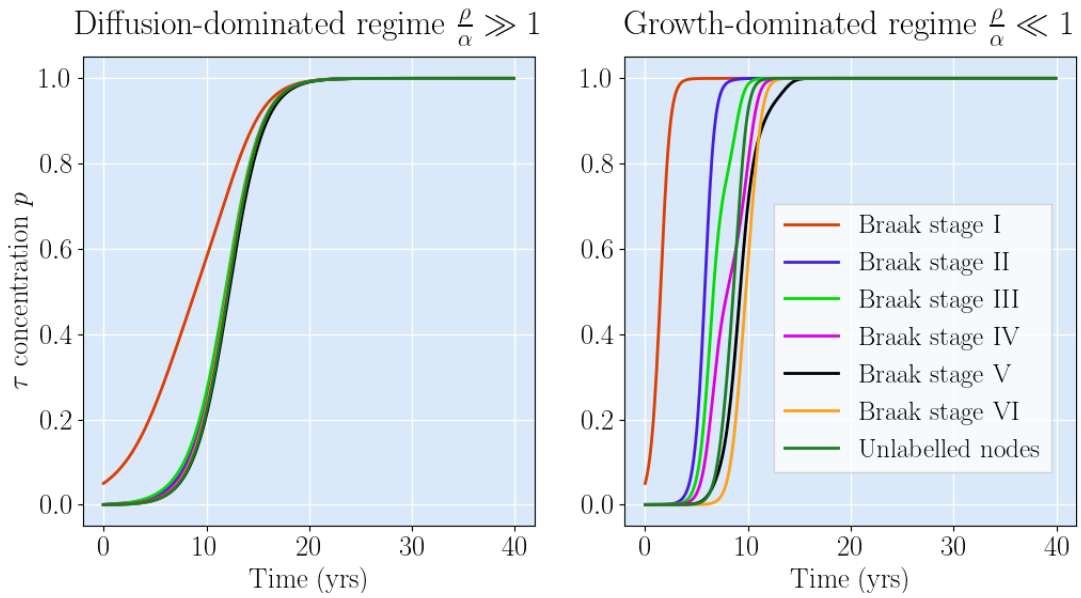

Figure 1: Average toxic τ concentration for the nodes grouped by Braak stage, for a growth-dominated regime with $\alpha = 0.6$ and $\rho = 3$ (left) and a diffusion-dominated one with $\alpha = 2.1$ and $\rho = 0.01$ (right).

times. Therefore, we know we must have that $\rho/\alpha \ll 1$, as in the right graph, where the Braak stages get activated one by one.

2.4 ANALYSIS

A steady state analysis shows that there are only two fixed points for the concentration of each node p_i in Equation (7). The healthy steady state $p_i = 0$ is an unstable one, only attained if the initial condition is $p_{i,0} = 0 \; \forall \, i$. As soon as any node has some nonzero initial seeding, the concentration of the misfolded proteins will converge toward the stable, toxic steady state $p_i = 1 \; \forall \, i$.

This is an unrealistic system: it implies that the misfolding of a single protein inevitably results in a full infection. However, random mutations and misfoldings are quite frequent in protein production in the brain without such an ominous outcome as the one predicted by this model. As mentioned earlier, we still have not accounted for the clearance mechanisms performed by the brain to dispose of general residues.

2.5 INSIGHT

Despite the simplicity of this model, it can play out as a good starting point valid for a wide range of neurodegenerative diseases. In the end, there are a number of them

considered to also spread in a prion-like manner, including Parkinson's disease and amyotrophic lateral sclerosis.

We can also use it to understand the connectivity between different brain regions. AD is known to start in the transentorhinal region, a poorly connected brain region. We can calculate the average concentration of all the nodes in the network for different initial seedings. We should expect that when the initial concentration is seeded on the transentorhinal region, it will take more time for the overall brain concentration to increase. In contrast, seeding the initial concentration in certain other regions will make the concentration increase faster.

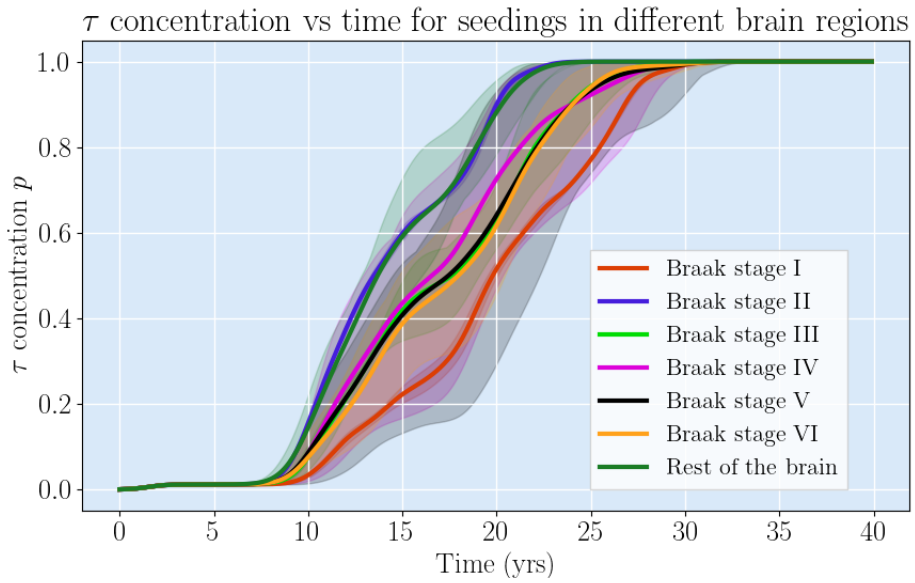

Figure 2: Average toxic τ concentration for the whole brain for initial concentration seeded in the different brain regions, coloured by association of the initial seeding location with the Braak stages.

We can confirm with Figure (2) that the nodes associated with Braak stage I are indeed poorly connected to the rest of the brain: when the misfoldings are seeded in those nodes, the time taken for the concentration to increase is longer than if it was seeded in any other brain region.

3 COUPLING CONCENTRATION WITH CLEARANCE

The way in which the clearance is modelled in this paper follows the model proposed in [10].

Including clearance should shift the previous stable, fully-saturated steady state to a lower concentration value, whereas the unstable, healthy steady state should remain where it was before. We also expect a transcritical bifurcation for these steady states as the clearance increases [14]. In other words, for high enough clearance levels the stability of the fixed points is interchanged, meaning the system will now converge to the healthy state thanks to the large clearance. A transcritical bifurcation for a parameter μ and a variable x looks like $\mu x - x^2$ when μ is close to 0. Therefore, if the critical value of the clearance is λ_{crit} and its value is $\lambda_i = \lambda_i(t)$ at node i, the bifurcation is

$$(\lambda_{crit} - \lambda_i)\, p_i - \alpha p_i^2, \tag{8}$$

where α regulates the population growth [14], as in Equation (1). Describing the diffusion with the Graph Laplacian as before, the concentration ODE follows from Equation (8):

$$\frac{\mathrm{d}p_i}{\mathrm{d}t} = -\rho \sum_{j=1}^{83} \frac{L_{ij} p_j}{v_i} + (\lambda_{crit} - \lambda_i) - \alpha p_i^2, \tag{9a}$$

$$p_i(0) = p_{i,0}. \tag{9b}$$

Given that we expect a decay in the clearance for increased concentration p, and assuming a global minimum clearance level of λ_{min} and a global kinetic constant β representing node vulnerability, the full model in [10] is:

$$\frac{\mathrm{d}p_i}{\mathrm{d}t} = -\rho \sum_{j=1}^{83} \frac{L_{ij} p_j}{v_i} + (\lambda_{crit} - \lambda_i) - \alpha p_i^2, \tag{10a}$$

$$\frac{\mathrm{d}\lambda_i}{\mathrm{d}t} = -\beta p_i \left(\lambda_i - \lambda_{min}\right), \tag{10b}$$

$$p_i(0) = p_{i,0}, \qquad \lambda_i(0) = \lambda_{i,0}. \tag{10c}$$

3.1 COMPUTATIONAL IMPLEMENTATION

Equations (10) can also be implemented using an explicit scheme. For simplicity, we will assume a homogeneous initial clearance: $\lambda_{i,0} = \lambda_0 \; \forall\, i$. However, with knowledge about the clearance levels for different brain regions, heterogeneous initial clearance levels can be set to achieve an increased accuracy. Initial concentration seeding will be set as before at those nodes associated with the first Braak stage.

Parameter values are displayed in Table (1) and are set to those used in [10]:

Table 1: Parameters for coupled model

Parameter	Value (yr^{-1})
ρ	0.01
α	2.1
λ_{crit}	0.72
λ_{min}	0.01
β	1

3.2 ANALYSIS

In this subsection, all parameters, including the initial concentration will be equal for all nodes. In this case, the system is equivalent to that of a single node. We will study the phase plane of only one node recalling that we are in a growth-dominated regime where diffusion has a lower relevance. We can formally ratify this approximation by considering ρ as a perturbation (due to its small value) and expanding [10]:

$$p_i(t) = p_{i,1} + \rho p_{i,2} + \mathcal{O}(\rho^2), \tag{11a}$$

$$\lambda_i(t) = \lambda_{i,1} + \rho \lambda_{i,2} + \mathcal{O}(\rho^2). \tag{11b}$$

These expansions can be substituted into Equation 10. The result, to leading-order, is:

$$\frac{\mathrm{d}p_{i,1}}{\mathrm{d}t} = (\lambda_{crit} - \lambda_{i,1})p_{i,1} - \alpha p_{i,1}^2, \tag{12a}$$

$$\frac{\mathrm{d}\lambda_{i,1}}{\mathrm{d}t} = -\beta p_{i,1}(\lambda_{i,1} - \lambda_{min}). \tag{12b}$$

This confirms that a single-node analysis disregarding the diffusion is not an unreasonable choice given the size of ρ.

3.2.1 BIFURCATION CURVE

As said earlier, for high enough clearance levels we expect the stability of the steady states to change, making the system converge to the healthy state. Hence, there is a curve in the concentration-clearance phase space separating the initial conditions where a healthy state is reached from those that converge to the unhealthy state. Also, we expect the concentration of the unhealthy steady state to have been lowered from its previous value of 1 due to the newly added clearance.

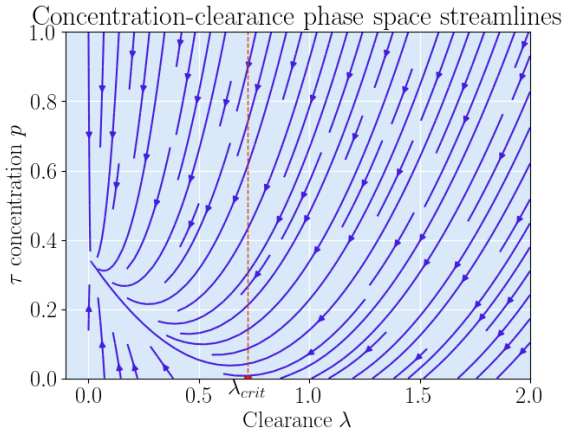

Figure 3: τ concentration vs clearance stream plot.

Trajectories on the phase space are shown in Figure (3). Indeed, the separating curve for the bifurcation can be deduced, together with the reduction in the concentration of the unhealthy steady state, which now seems to be near 0.3.

It is crucial to understand the conditions of the bifurcation curve and find it, given that it makes the difference between the system getting infected or not. With that motivation we can parametrise the curve $p_{crit}(\lambda)$ as that trajectory which, with initial conditions $p_0 = p_{crit}(\lambda_0)$ and λ_0, intersects the horizontal axis at $p(\lambda_{crit}) = 0$. We can remove the time dependence from the equations by dividing Equation (12a) by Equation (12b):

$$\frac{\partial p}{\partial \lambda} = -\frac{\lambda_{crit} - \lambda - \alpha p}{\beta\,(\lambda - \lambda_{min})} = \frac{\alpha}{\beta}\frac{p}{\lambda - \lambda_{min}} - \frac{\lambda_{crit} - \lambda}{\beta(\lambda - \lambda_{min})}. \tag{13}$$

Rearranging and multiplying by $(\lambda - \lambda_{min})^{-\alpha/\beta}$:

$$(\lambda - \lambda_{min})^{-\alpha/\beta}\frac{\partial p}{\partial \lambda} - \frac{\alpha}{\beta}(\lambda - \lambda_{min})^{-\alpha/\beta - 1}p = \frac{\lambda - \lambda_{crit}}{\beta(\lambda - \lambda_{min})^{\alpha/\beta + 1}}. \tag{14}$$

Notice it can be expressed as an exact ODE:

$$\frac{\partial}{\partial \lambda}\left[\frac{p}{(\lambda - \lambda_{min})^{\alpha/\beta}}\right] = \frac{\lambda - \lambda_{crit}}{\beta(\lambda - \lambda_{min})^{\alpha/\beta + 1}}. \tag{15}$$

Integrating Equation (15) from $(p_0,\, \lambda_0)$ to $(0,\, \lambda_{crit})$ by parts and then solving for p_0 gives:

$$p_0 = \frac{\alpha(\lambda_{crit} - \lambda_0) + \beta(\lambda_{min} - \lambda_{crit}) + \beta(\lambda_0 - \lambda_{min})^{\alpha/\beta}(\lambda_{crit} - \lambda_{min})^{1-\alpha/\beta}}{\alpha(\alpha - \beta)}. \tag{16}$$

Equation (16) shows the initial concentration at which the bifurcation occurs for every λ_0. This result can be tested by numerically solving the equations for different

initial conditions. We will choose $\lambda_0 = 1$, with a corresponding $p_0 \approx 0.056$, and also plot the trajectories of $p_0 \pm 0.01$.

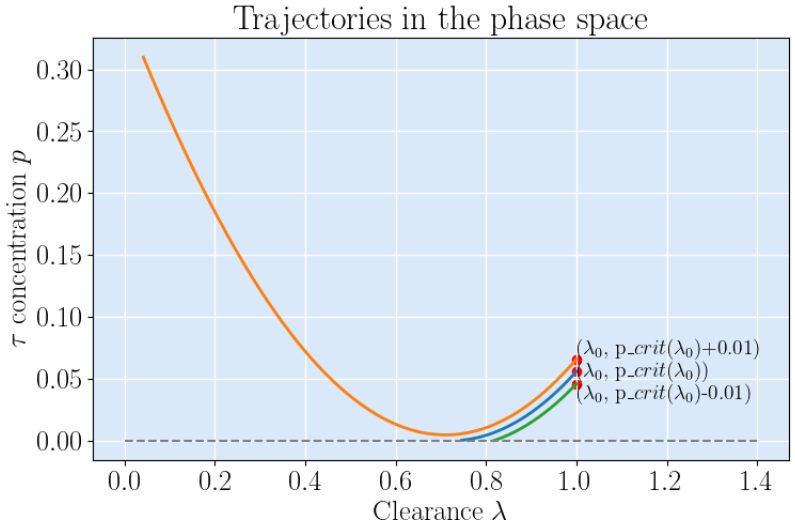

Figure 4: τ concentration vs clearance phase plane trajectories.

Figure (4) shows that, as expected, any state with initial conditions (λ_0, p_0) converges to the unhealthy steady state $\forall\, p_0 > p_{crit}(\lambda_0)$ and to the healthy state $\forall\, p_0 < p_{crit}(\lambda_0)$.

3.2.2 REDUCED CONCENTRATION FOR THE UNHEALTHY STEADY STATE

As noted earlier and as confirmed by Figures (3) and (4), the unhealthy steady state has a concentration lower than one. Now, finding out how much it has decreased can also provide insight into the system dynamics with the coupled clearance. Setting Equations (12a) and (12b) equal to 0, we find that $(\lambda, p) = (\lambda_{min}, \frac{\lambda_{crit} - \lambda_{min}}{\alpha})$ are its coordinates in the phase plane, so a concentration of around 0.338, almost three times lower than without clearance.

3.2.3 NETWORK CONNECTIVITY

Even though diffusion is small, we can quantify how it affects the evolution of the clearance level. For this, we will model an unweighted star network with one central node and N peripheral nodes, where the only connections are from the central node to the rest. For it to be unweighted, we make the adjacency matrix entries be 1 for those

nodes that do have a connection, which yields a different Graph Laplacian through an analogous procedure as the one done before.

Now, the final clearance reached by the system for every initial seeding value in the central node can be plotted as a continuous line. Furthermore, we can plot several of these lines for networks with a different number N of peripheral nodes.

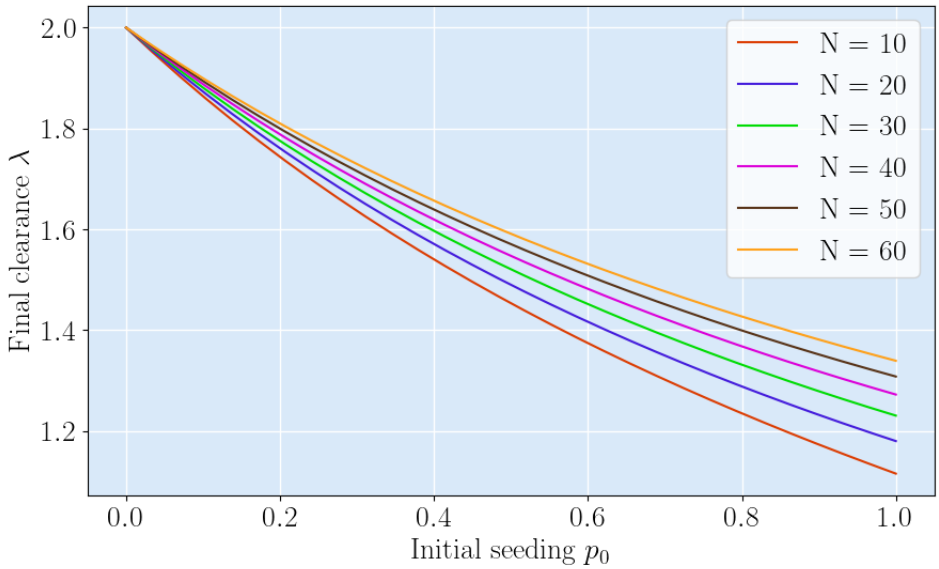

Figure 5: Final clearance vs initial seeding for different numbers of peripheral nodes in an unweighted star network, with $\lambda_0 = 2$ and the rest of parameters as in Table (1).

The results are displayed in Figure (5). Notice how a bigger number of nodes means a larger final clearance attained for the same initial seeding. In other words, diffusion helps redistributing the misfolded τ concentration so that it is easier for the clearance mechanisms to remove it.

All in all, implementing clearance as a first order law has reduced the saturation concentration by almost three times compared to the Fisher-KPP model without clearance. Hence, we can conclude that this model is a much more realistic one that aligns better with the way AD spreads. It allows for small concentrations of misfolded τ proteins to be fully removed, which is a basic mechanism for survival that was not present in the previous model.

4 DAMAGE

As an extension, we can try to also account for the damage in the neural connections as the disease progresses. We parametrise damage as an independent variable $q \in [0, 1]$ which evolves according to its own ODE. When damage is 1 in two connected nodes, we expect their connectivity to drop to 0. The extended system we propose is:

$$\frac{\mathrm{d}p_i}{\mathrm{d}t} = -\rho \sum_{j=1}^{83} \frac{\tilde{L}_{ij}(q_i, q_j)p_j}{v_i} + (\lambda_{crit} - \lambda_i) - \alpha p_i^2, \tag{17a}$$

$$\frac{\mathrm{d}\lambda_i}{\mathrm{d}t} = -\beta p_i \left(\lambda_i - \lambda_{min}\right), \tag{17b}$$

$$\frac{\mathrm{d}q_i}{\mathrm{d}t} = \beta p_i (1 - q_i), \tag{17c}$$

$$p_i(0) = p_{i,0}, \qquad \lambda_i(0) = \lambda_{i,0}, \qquad q_i(0) = 0, \tag{17d}$$

where now the entries in the Graph Laplacian decay with the damage of the two nodes it connects. This will have the effect of reducing, if not completely eliminating diffusion as τ concentration increases.

We propose a linear and an exponential dependence of the Graph Laplacian on damage:

$$\tilde{L}_{ij}(q_i, q_j) = L_{ij} \cdot \frac{2 - q_i - q_j}{2}, \tag{18a}$$

$$\tilde{L}_{ij}(q_i, q_j) = L_{ij} \cdot \max\left\{ \frac{e^{2\kappa - q_i - q_j}}{e^{2\kappa} - 1}, 0 \right\}, \tag{18b}$$

where $\kappa \in (0, 1)$ should be chosen to adjust the connectivity deterioration due to damage.

The evolution of the Laplacian can be visualised using heatmaps, as in Figures (6) and (7). We see that over a period of 60 years, the linear decrease of the connectivity with damage completely destroys all neural connections between nodes, while the exponential does not lead them to 0. However, after 30 years the exponential has inflicted more damage than the linear. This makes the model even more realistic and creates new steady states with lower τ concentration for the later Braak stages, as shown in Figure (8).

This result, one the one hand, helps preventing a higher concentration load from reaching certain areas of the brain. However, it does so at the cost of deteriorating the neural connections, and therefore impeding the spread of the misfolded proteins.

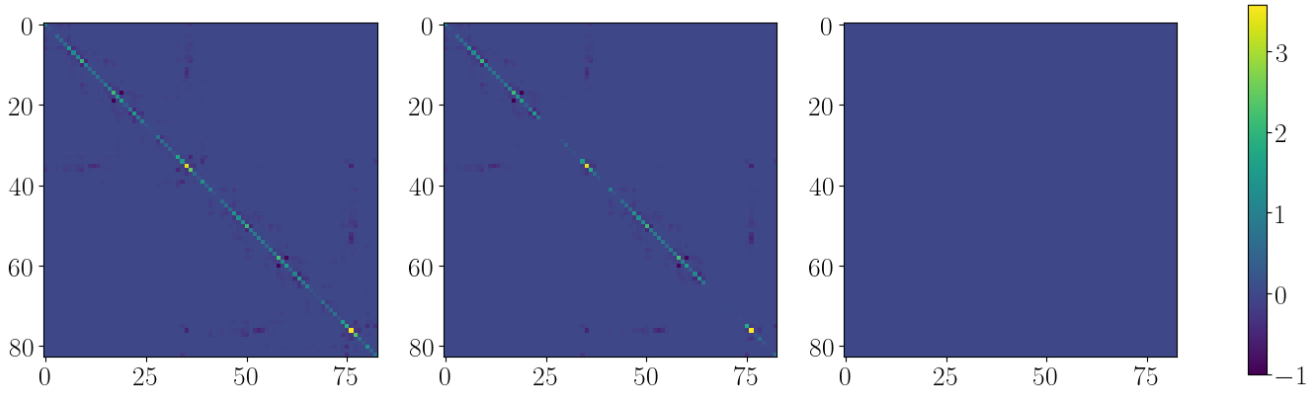

Figure 6: Laplacian heatmap with linear dependence on damage for different points in time: $t = 0$ (left), $t = 30$ (centre), $t = 60$ (right).

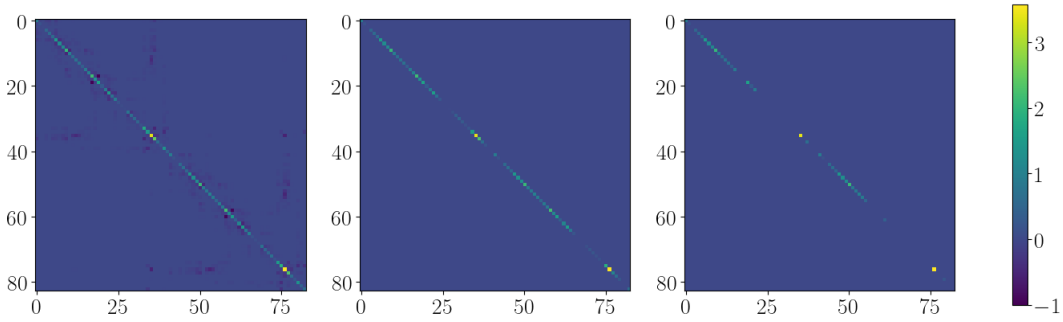

Figure 7: Laplacian heatmap with exponential dependence on damage for different points in time: $t = 0$ (left), $t = 30$ (centre), $t = 60$ (right). Here, $\kappa = 0.9$.

We can now compare all the different models developed on this study with the parameters shown in Table (1) together with $\kappa = 0.9$. Initial conditions will be $\lambda_0 = 0.1$ and $q_0 = 0$ for all nodes, and $p_0 = 0.2$ for those nodes belonging to the transentorhinal region as before.

Looking at the concentration curves for the new damage model in Figure (8) we can see that both linear and exponential connectivity damage delay the progression of Alzheimer's by a small amount. Moreover, with a closer look we see that the exponential damage not only delays the infection, but also decreases the steady state concentration of the Braak stages IV, V, VI, and the unlabelled nodes.

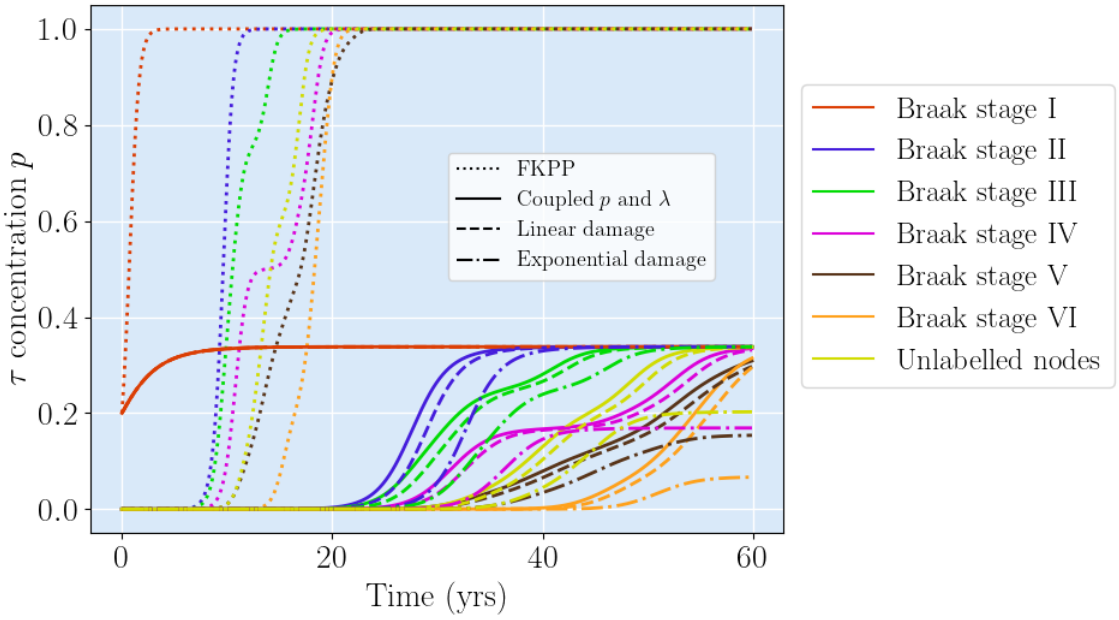

Figure 8: Toxic τ concentration vs time for all the models studied.

5 Conclusion

This case study has given a huge perspective in understanding the progression of Alzheimer's Disease by using the prion hypothesis applied to τ proteins. Through meticulous simulations using the Fisher-KPP model, and subsequent models incorporating brain clearance and damage mechanisms, the study provides crucial insights into the mechanisms of neurodegeneration in AD.

Initially, the Fisher-KPP model offered a basic framework for tracking the diffusion and interaction of misfolded τ proteins within the brain's connectome. The model's ability to predict the spread of toxicity through neural pathways highlights its utility in mapping progression of different prion-like diseases. However, modifying this model to include brain clearance mechanisms significantly improved our understanding by depicting how neurodegenerative processes might be mitigated or exacerbated by the brain's responses to accumulating proteins.

Subsequently, the inclusion of brain damage in the model allowed for a more comprehensive understanding of the disease's progression and its impact on neural connectivity. The analysis revealed that damage not only restricts the spread of misfolded proteins but also alters the overall connectivity within the brain, suggesting that the deterioration of neural pathways does indeed have a significant effect on the evolution of the disease.

The mathematical models explored in this study, particularly those integrating clearance and damage mechanisms, highlight the complex interplay between biological processes at the molecular level. These models suggest potential therapeutic targets aimed at improving clearance mechanisms or protecting neural connectivity, which could pave the way for interventions that delay or mitigate the progression of AD.

This study not only reinforces the importance of mathematical models in biomedical research but also provides a baseline for future studies to explore other neurodegenerative diseases using similar methodologies. As our understanding of the underlying biological processes improves, so too will our ability to intervene and alter the course of neurodegenerative diseases. The refinement of these models, informed by emerging clinical insights, promises to unlock new possibilities in the prevention and treatment of neurodegenerative disorders, potentially leading to breakthroughs in how these illnesses are managed in clinical settings.

References

[1] Alzheimer's Disease International. "Dementia statistics." (2020), [Online]. Available: https://www.alzint.org/about/dementia-facts-figures/dementia-statistics/#:~:text=There%20are%20over%2055%20million,and%20139%20million%20in%202050. (visited on 04/24/2024).

[2] S. B. Prusiner, "Some speculations about prions, amyloid, and alzheimer's disease," *The New England Journal of Medicine*, vol. 310, no. 10, pp. 661–663, 1984. DOI: 10.1056/NEJM198403083101021.

[3] J. Ma and F. Wang, "Prion disease and the 'protein-only hypothesis'," *Essays in Biochemistry*, vol. 56, pp. 181–191, 2014. DOI: 10.1042/bse0560181.

[4] G. G. Glenner, "On causative theories in alzheimer's disease," *Human Pathology*, vol. 16, no. 5, pp. 433–435, 1985. DOI: 10.1016/s0046-8177(85)80078-2.

[5] W. Gulisano *et al.*, "Role of amyloid- and tau proteins in alzheimer's disease: Confuting the amyloid cascade," *Journal of Alzheimer's Disease*, vol. 64, no. s1, S611–S631, 2018. DOI: 10.3233/JAD-179935.

[6] C. Kerepesi, B. Szalkai, B. Varga, and V. Grolmusz, "The braingraph.org database of high resolution structural connectomes and the brain graph tools," *Cognitive Neurodynamics*, vol. 11, no. 5, pp. 483–486, 2017. DOI: 10.1007/s11571-017-9445-1.

[7] H. Braak and K. D. Tredici, "Evolutional aspects of alzheimer's disease pathogenesis," *Journal of Alzheimer's Disease*, vol. 33, S155–S161, 2013. DOI: 10.3233/JAD-2012-129029.

[8] R. A. Fisher, "The wave of advance of advantageous genes," *Annals of Eugenics*, vol. 7, pp. 355–369, 1937. DOI: 10.1111/j.1469-1809.1937.tb02153.x.

[9] A. N. Kolmogorov, "A study of the equation of diffusion with increase in the quantity of matter, and its application to a biological problem," *Moscow Univ. Bull. Math.*, vol. 1, pp. 1–25, 1937.

[10] G. S. Brennan, T. B. Thompson, H. Oliveri, M. E. Rognes, and A. Goriely, "The role of clearance in neurodegenerative diseases," *SIAM Journal on Applied Mathematics*, vol. 0, no. 0, S172–S198, 2023. DOI: 10.1137/22M1487801.

[11] Q. Huang and M. E. Figueiredo-Pereira, "Ubiquitin/proteasome pathway impairment in neurodegeneration: Therapeutic implications," *Apoptosis*, vol. 15, pp. 1292–1311, 2010. DOI: 10.1007/s10495-010-0466-z.

[12] J. M. Tarasoff-Conway *et al.*, "Clearance systems in the brain - implications for alzheimer disease," *Nature Reviews Neurology*, vol. 11, pp. 457–470, 2015. DOI: 10.1038/nrneurol.2015.119.

[13] S. Fornari, A. Schäfer, M. Jucker, A. Goriely, and E. Kuhl, "Prion-like spreading of alzheimer's disease within the brain's connectome," *Journal of The Royal Society Interface*, vol. 16, no. 159, p. 20 190 356, 2019. DOI: 10.1098/rsif.2019.0356.

[14] T. B. Thompson, G. Meisl, T. P. J. Knowles, and A. Goriely, "The role of clearance mechanisms in the kinetics of pathological protein aggregation involved in neurodegenerative diseases," *The Journal of Chemical Physics*, vol. 154, p. 125 101, 2021. DOI: 10.1063/5.0031650.